

Electrospun Antibacterial Composites for Cartilage Tissue Engineering

Muhammad Samie,* Ather Farooq Khan, John George Hardy,*
and Muhammad Arfat Yameen

Implantation of biomaterials capable of the controlled release of antibacterials during articular cartilage repair may prevent postoperative infections. Herein, biomaterials are prepared with biomimetic architectures (nonwoven mats of fibers) via electrospinning that are composed of poly(ϵ -caprolactone), poly(lactic acid), and *Bombyx mori* silk fibroin (with varying ratios) and, optionally, an antibiotic drug (cefixime trihydrate). The composition, morphology, and mechanical properties of the nanofibrous mats are characterized using scanning electron microscope, Fourier transform infrared spectroscopy, and tensile testing. The nonwoven mats have nanoscale fibers (typical diameters of 324–725 nm) and are capable of controlling the release profiles of the drug, with antibacterial activity against Gram +ve and Gram –ve bacteria (two common strains of human pathogenic bacteria, *Staphylococcus aureus* and *Escherichia coli*) under in vitro static conditions. The drug loaded nanofiber mats display cytocompatibility comparable to pure poly(ϵ -caprolactone) nanofibers when cultured with National Institutes of Health (NIH) NIH-3T3 fibroblast cell line and have long-term potential for clinical applications in the field of pharmaceutical sciences.

joint), hence it is challenging to deal with an injured cartilage. Sometimes the problem gets worsened due to the development of infections if not treated early or if the patient is diabetic.^[1,2] The success rate of in practice traditional clinical therapies (i.e., autografting, allografting and autologous chondrocyte implantation) is still very low because of the associated complications such as donor site morbidity, nonavailability of the grafted tissue for larger defects, and immune reactions.^[3] Tailoring the properties of natural and synthetic polymer-based biomaterials is impactful for biomedical applications including drug delivery and tissue engineering,^[4–8] for example biomaterials for cartilage regeneration.^[9–11]

Fibrous tissue scaffolds prepared via electrospinning resemble the fibers/fibrils in naturally occurring extracellular matrix (ECM) and have received significant attention in cartilage tissue repair research.^[12,13] Mats of electrospun

nanofibers have been utilized for a variety of biomedical applications, including biosensors,^[14] drug delivery systems,^[15] wound dressings,^[16] and tissue scaffolds.^[17] The tendency of such mats to have highly porous 3D architectures, with high surface area to volume ratios is beneficial for cell proliferation and transport of nutrients/waste to/from cells inhabiting them, making them interesting candidates for cartilage repair.^[18]

Encapsulation of drugs inside a polymer matrix enables the scaffolds to increase the residence time of the drug through

1. Introduction

Cartilage defects are one of the most common clinical problems resulting from accidents, osteoarthritis, aging, and other metabolic disorders. Cartilage tissue is mechanically robust yet limited ability to naturally repair itself due to its avascular nature. During the movement of joints cartilage tissue is continuously exposed to frictional forces (especially in the weight bearing


M. Samie, A. F. Khan
Interdisciplinary Research Centre in Biomedical Materials
COMSATS University Islamabad
Lahore campus, Lahore 54000, Pakistan
E-mail: muhammadsamie@cuilahore.edu.pk

M. Samie, M. A. Yameen
Department of Pharmacy
COMSATS University Islamabad
Abbottabad campus, Abbottabad, Khyber Pakhtunkhwa 22060, Pakistan

M. Samie, J. G. Hardy
Department of Chemistry
Lancaster University
Lancaster, Lancashire LA1 4YB, UK
E-mail: j.g.hardy@lancaster.ac.uk

M. Samie, J. G. Hardy
Materials Science Institute
Lancaster University
Lancaster, Lancashire LA1 4YB, UK

M. Samie
Institute of Pharmaceutical Sciences
Khyber Medical University
Peshawar, Khyber Pakhtunkhwa 25100, Pakistan

 The ORCID identification number(s) for the author(s) of this article can be found under <https://doi.org/10.1002/mabi.202200219>

© 2022 The Authors. Macromolecular Bioscience published by Wiley-VCH GmbH. This is an open access article under the terms of the Creative Commons Attribution License, which permits use, distribution and reproduction in any medium, provided the original work is properly cited.

DOI: 10.1002/mabi.202200219

sustained release at the site of implant^[19] and electrospinning provides great flexibility in producing materials capable of prolonged drug release for drugs/therapeutics of various molecular weights (including proteins, vitamins, and antibiotics) incorporated inside unicomponent, multicomponent, uniaxial, or coaxial electrospun nanofibers.^[20]

Aliphatic polyesters are degradable polymers that are often used in regenerative medicine.^[21,22] Among these, poly(ϵ -caprolactone) (PCL) and poly(lactic acid) (PLA), are widely explored for tissue engineering applications such as bone regeneration,^[23,24] dental regeneration,^[25] cardiac regeneration,^[26] and vascular regeneration,^[27] both alone and as composites. However, most of the research using both polymers in the form of blends/composites was focused on applications other than cartilage tissue engineering. Research has highlighted the osteogenic and chondrogenic potential of electrospun PCL and PLA nanofiber mats,^[28,29] supporting exploration as cartilage tissue scaffolds.

The use of natural materials in fabrication of nanofibers for drug delivery and tissue engineering applications is becoming increasingly popular.^[30–34] *Bombyx mori* silk fibroin (SF) is a biopolymer that can be processed into materials with a variety of morphologies which is useful for drug delivery and tissue engineering applications,^[35–39] alone or indeed as composites.^[40,41]

Cefixime trihydrate (CFX) is a broad-spectrum antibiotic with very low aqueous solubility that is commonly used in postsurgical therapies.^[42] Here we report the results of investigating CFX-loaded nanofibers fabricated by electrospinning mixtures of PCL, PLA, and SF in different weight ratios. The nanofiber mats were evaluated using scanning electron microscopy, Fourier-transform infrared spectroscopy, mechanical testing, and water contact angle measurements. The opportunity to use such biomaterials was validated in vitro via CFX release profile measurements, antibacterial efficiency estimated via the disc diffusion and turbidimetric methods, and the adhesion and proliferation of National Institutes of Health (NIH) NIH-3T3 fibroblast cells was assessed by the MTT/live–dead assays and electron microscopy.

2. Experimental Section

2.1. Chemicals

PCL MW 80 000 was purchased from Sigma-Aldrich (St. Louis, MO). Degummed SF fibers (throwsters waste) were purchased from Etsy. Cefixime trihydrate was received as gift sample from Al-Sayed Pharma Hattar, Pakistan. Methanol was acquired from Daejung (Chemical and Metals Co. Ltd., Korea). Dichloromethane (DCM) was procured from Tedia company Inc. USA. Nutrient agar was purchased from OXOID Ltd, Basingstoke, Hampshire, England. LB (Luria-Bertani) broth was purchased from Scharlab, S.L, Barcelona, Spain. Bacterial strains were obtained from American Type Culture Collection (*S. aureus*: ATCC-6538, *E. coli*: ATCC-25922). NIH-3T3 fibroblast cell line was from American type culture collection (ATCC: CRL-6442). Dulbecco's Modified Eagle's Medium (DMEM) was obtained from Gibco, Life Technologies, USA. Fetal bovine serum and penicillin/streptomycin were obtained from Caisson, USA. Phosphate buffer saline tablets (pH 7.4) from BioPLUS™ Fine Research Chemicals and MTT assay kit was purchased from

Table 1. Composition of the developed formulations and experimental conditions.

Sample number	Polymer [wt%]				Electrospinning conditions
	PCL	PLA	SF	CFX	
S1	100	–	–	–	17 kV, 10 cm, 1.5 mL h ⁻¹
S2	100	–	–	20	17 kV, 10 cm, 1.5 mL h ⁻¹
S3	–	100	–	20	17 kV, 10 cm, 1.5 mL h ⁻¹
S4	50	50	–	20	17 kV, 10 cm, 1.5 mL h ⁻¹
S5	50	–	50	20	17 kV, 10 cm, 1.5 mL h ⁻¹
S6	–	50	50	20	17 kV, 10 cm, 1.5 mL h ⁻¹

Chemicon (Cat No. CT01-5). All other chemicals used were of analytical grade.

2.2. Electrospinning

The electrospinning process for fabrication of uniaxial controlled release nanofiber mats was carried out under constant working conditions such as applied voltage, flow rate, and tip-to-collector distance. Briefly, PCL and PLA were dissolved in a mixture of dichloromethane and methanol (3:2, v/v), whereas SF was dissolved in 1,1,1,3,3,3-hexafluoro-2-propanol in a closed container with the help of magnetic stirrer (6 h, at room temperature). The model drug was then mixed with the polymer solution in such a way that the final solution contains 20% w/w CFX of the total polymer contents that was kept as 15% (Table 1). The polymer-drug blend was then loaded into a plastic syringe equipped with a 23-gauge blunt end needle and fixed in place in a syringe pump. An applied electric current of 17 kV and ejection rate of 1.5 mL h⁻¹ were selected for the electrospinning process. The nanofibers were collected on a nonstick aluminum foil wrapped on a rotating drum kept at distance of 10 cm from the tip of needle. Keeping in view the conventional postoperative treatment duration, the experimental design of experiments undertaken in the study was set to 7 d.

2.3. Scanning Electron Microscopy

The surface morphology of CFX-loaded nanofiber mats was examined with the help of scanning electron microscope (SEM, VEGA3, Tescan) after gold sputtering. The average diameter of nanofibers was calculated using Image J software. The diameter of at least 30 fibers was measured randomly and the mean and standard deviations were plotted. Similarly, the pore size was calculated by measuring the average of vertical and horizontal pore dimensions.

2.4. Fourier Transform Infrared (FT-IR) Spectroscopy

The nature of possible interactions between polymer and drug and the appearance of different surface functional groups were studied through FT-IR spectroscopy under attenuated total reflectance mode within the range of 4000–650 cm⁻¹ using FT-IR

Table 2. Correlation between contact angle and nature of formulation.

Contact angle	Nature
<30°	Hydrophilic
<10°	Super-hydrophilic
90°–120°	Hydrophobic
>150°	Super-hydrophobic

Thermo Fisher scientific (Nicolet-6700, USA) at room temperature. A total of 128 scans were run for each sample with a resolution of 8 cm⁻¹ after nitrogen purging.

2.5. Mechanical Properties

The ultimate tensile strength of nanofiber sheets in dry state according to the American Society for Testing and Materials (ASTM) D5024-95a guidelines was measured with the help of electrodynamic fatigue testing machine (LFV-E 1.5 kN). The nanofiber sheets were cut into elongated strips of 30×5×0.03 mm³ (L × W × T) dimensions. The strips were fixed vertically between the grips and the force was applied at a displacement rate of 1 mm min⁻¹.^[43]

2.6. Water Contact Angle Measurement

The angle formed between the liquid droplet and nanofibers surface was measured by putting a 10 µL drop of distilled water on the nanofibers sheet placed on a flat surface. The images were recorded over a period of few seconds using a microcapture camera and further processed for measuring the contact angle using image J software.^[44] The spreadability of water on a surface describes its hydrophilic or hydrophobic nature. **Table 2** presents the nature of a material with respect to its contact angle.^[45]

2.7. In Vitro Release of Cefixime Trihydrate

The release profile of CFX from the developed nanofiber mats in dissolution medium was estimated by measuring the drug concentration in the release medium using UV-vis spectrophotometer (Perkin Elmer's Lambda 25). Briefly the nanofiber sheets were cut into rectangular pieces in such a way that it contains an equivalent amount of drug and put in 10 mL phosphate buffered saline (PBS) solution (pH 7.4) maintained at 37 °C. After each time point 1 mL aliquot from the dissolution medium was withdrawn and the absorbance was measured at 287 nm through UV-vis spectrophotometer. After each withdrawal an equal amount of fresh PBS was replenished to the dissolution medium in order to maintain the fluid volume constant. The cumulative drug release was then calculated from the previously plotted standard curve data and the obtained data were fitted into various kinetic models to explore the mechanism of drug release from the electrospun nanofiber mats.^[46]

2.8. In Vitro Antibacterial Study

Two most common human pathogenic bacteria *Escherichia coli* ATCC No. 25922 (Gram-negative) and *Staphylococcus aureus* ATCC No. 6538 (Gram-positive) were used as test organisms in the study. The antibacterial activity of CFX-loaded electrospun nanofiber mats was measured quantitatively through turbidimetric method and qualitatively via the disc diffusion method.

2.8.1. Turbidimetric Method

Briefly, bacterial cultures of the microorganisms were made in LB broth with an absorbance value of 0.1–0.2 measured at a wavelength of 625 nm with UV-visible spectrophotometer in order to have an optimal number of bacteria. 5 mL of this solution was added to individual 15 mL glass tubes and CFX-loaded nanofiber mats were added to each test tube. CFX powder was used as positive control while blank PCL nanofibers were used as negative control. All the samples were run in triplicate and incubated at 37 °C in a shaking incubator at 100 rpm for 24 h.^[47] After incubation, the optical density (OD) value was again measured and the percentage bacterial inhibition was calculated from the following equation

$$\% \text{ Bacterial inhibition} = \frac{I_c - I_s}{I_c} \times 100 \quad (1)$$

where I_c and I_s represent the mean ODs of the negative control and investigational groups, respectively.

2.8.2. Disc Diffusion/Kirby-Bauer Method

CFX-loaded nanofiber sheets were shaped into circular discs of 5 mm diameter. Petri plates were filled up to the mark with sterilized nutrient agar media and left to solidify. 50 µL of bacterial suspension with an OD value of 0.1–0.2 measured at 625 nm for each type of bacteria was streaked over the prepared solidified agar plates. Nanofiber discs were added to the plate surfaces under aseptic conditions. The plates were then incubated at 37 °C for 24 h. The clear zones formed around the discs were measured and recorded.^[48]

2.9. Cytocompatibility Assay through MTT of the Medicated Nanofiber Mats

The traditional MTT cell viability assay was conducted to measure the cytotoxicity of prepared nanofiber mats against NIH-3T3 fibroblast cell lines. MTT works on assessing the mitochondrial ability or cellular metabolism by measuring the intensity of purple color that results from the catalysis/reduction of MTT reagent to formazan by mitochondrial dehydrogenase enzyme over time. Briefly, circular discs of the nanofiber mats were cut and sterilized in UV light for 30 min. The nanofiber discs were then placed individually in each well of the well plates. Precultured NIH-3T3 cells in DMEM supplemented with 10% fetal bovine serum (FBS) and 1% penicillin-streptomycin were seeded

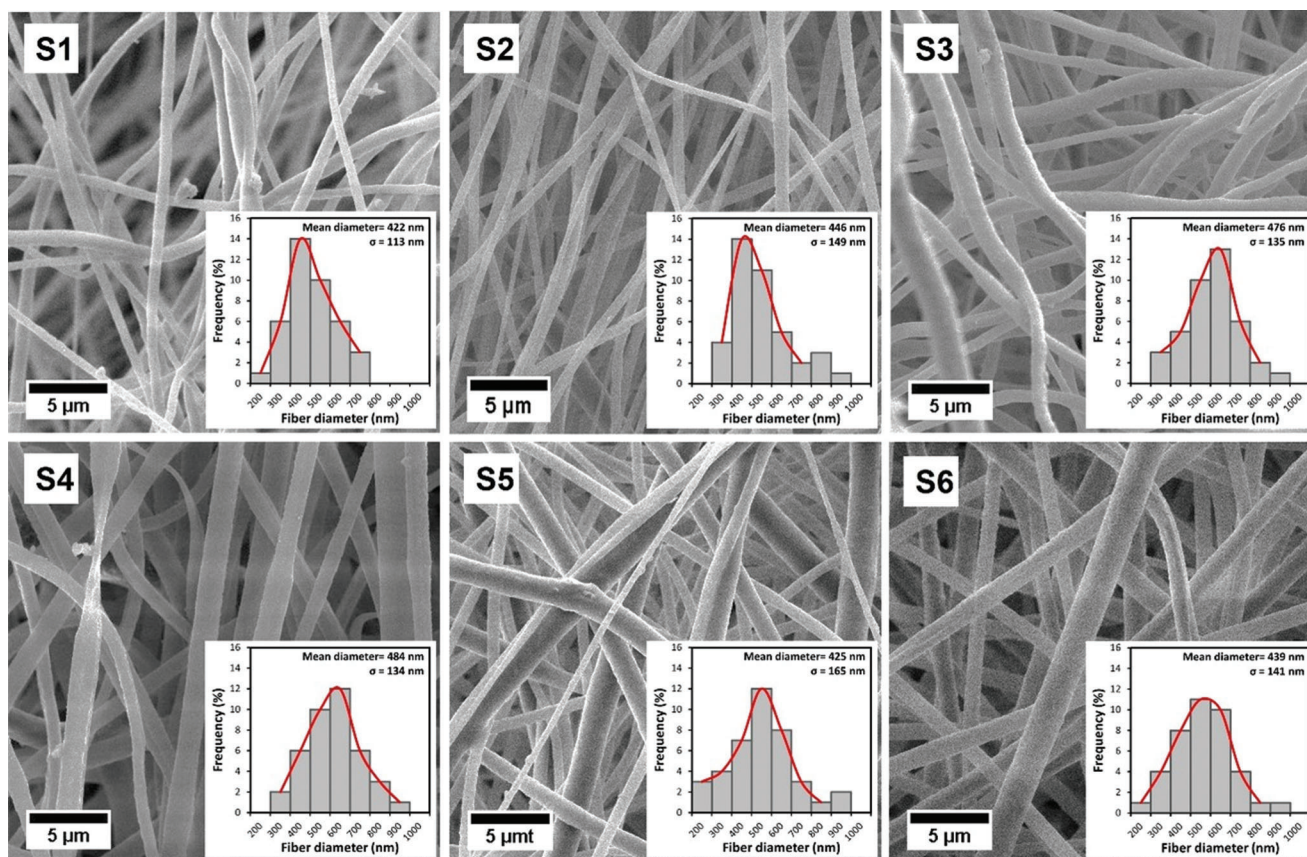


Figure 1. SEM photographs and fiber size distribution of the electrospun mats (S1–S6). Scale bars represent 5 μm .

at a concentration/density of 1×10^4 cells per well. The plates were then maintained in an incubator with 5% CO_2 at 37 $^\circ\text{C}$ for 1 and 3 d. After day 1 and day 3, the culture medium was aspirated and 100 μL of MTT reagent (3-[4,5-dimethylthiazol-2-yl]-2,5-diphenyltetrazolium bromide) was added to each well and incubated for 4 h in dark. The absorbance was measured at a wavelength of 595 nm with the help of Biorad PR4100 absorbance microplate reader using empty tissue culture plate as control. The discs after being cultured for 3 d were washed to remove any debris and fixed for observing the morphology under SEM.^[49]

2.10. Cell Attachment Assay

A density of 2×10^4 cells per well of the exponentially growing cells were seeded on the nanofiber sheets in a 24 well plate. The seeding step was followed by incubation at 37 $^\circ\text{C}$ in a CO_2 incubator in order to allow the cells to attach and infiltrate inside the electrospun mats. At the end of incubation (after 3 d) the plates were carefully washed three times using sterile PBS and then fixed by treating with 4% paraformaldehyde (PFA) solution for 30 min. The samples were again washed with cell culture grade PBS and dehydrated using a graded series of diluted alcohol, i.e., 50%, 60%, 70%, 80%, 90%, and 100% followed by drying in air inside a fume hood. The samples were then analyzed using SEM.^[44]

2.11. Live–Dead Assay

A live–dead assay was performed to differentiate between viable and nonviable cells. NIH-3T3 cells at a density of 2×10^4 cells per well were seeded on the samples and incubated for 3 d in a CO_2 incubator. The cells were then carefully washed with sterile PBS and added with calcein acetoxyethyl ester (AM) and propidium iodide to let the viable cells fluoresce green and dead as red color respectively under fluorescence microscope.

3. Results and Discussion

3.1. Materials Characterization

The SEM images are showing ultrafine nanofibers with a nonwoven structure of all the formulations as shown in **Figure 1**. Nanofibers with cylindrical morphologies and smooth surfaces can be seen in case of PCL, PLA, and their blend which is in accordance with the findings of nanofibers produced by electrospinning.^[50] The nanofiber mats exhibited variable pore sizes and geometry. Sample S1 and S2 had a mean diameter of 422 ± 113 and 446 ± 149 nm and an average pore diameter of 863 ± 142 and 925 ± 124 nm, respectively. A similarly smooth surface morphology was observed in the case of CFX-loaded PLA (S3) and PCL/PLA composite mats (S4) was observed, in line with the literature.^[51] In a previously reported study, the PCL and PLA at a concentration of 50/50 was considered as optimum for load-

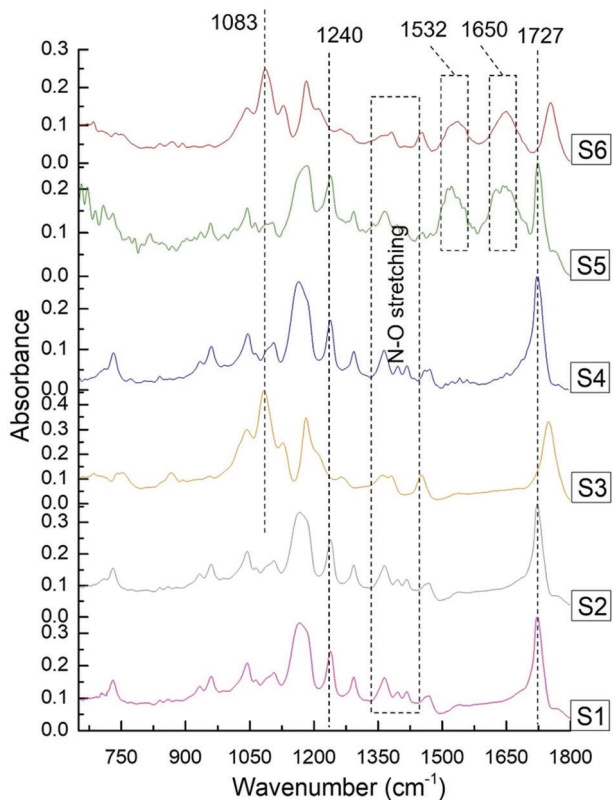


Figure 2. FT-IR spectrum of the nanofiber formulations (S1–S6).

ing 15% of the model drug tetracycline hydrochloride for wound healing applications.^[48] Loading of 20% drug in our case resulted in PCL/PLA composite nanofibers (S4) with mean diameters of 484 ± 134 nm. In contrast, samples containing SF, i.e., S5 and S6 have resulted in some fibers having flattened morphology. The nanofibers are arranged in a compact structure with uniform diameter along their length and the crossing points do not display melt fusion between the fibers without solid aggregates or bead formation. Comparing the average diameter of PCL/PLA composite nanofibers the average fiber diameter of S5 and S6 were estimated to be 425 ± 165 and 439 ± 141 nm, respectively, with pore diameters of 986 ± 158 and 911 ± 126 nm, respectively. The subtle differences in fiber diameter can be attributed to the difference in conductivity of both the solvents used in the solvent system. The incompatibility of SF with PCL and PLA is an obstacle, however, the solvent system has overcome this obstacle.^[34,52] The PCL/SF and PLA/SF nanofiber mats are somewhat hydrophilic because of the presence of hydrophilic domains in the SF structure.

The FT-IR spectra of the nanofiber mats (**Figure 2**) offer insights into their compositions. The vibration bands corresponding to C=O stretching at 1727 cm^{-1} , C–O–C stretching at 1293 and 1240 cm^{-1} , and C–O stretching at 1168 cm^{-1} in case of formulations S2, S4, and S5 are from PCL that exhibits representative peaks at 1760 , 1297 , 1238 , and 1168 cm^{-1} ; the presence of these peaks confirms the presence of PCL. Similarly, the presence of PLA in formulations S3, S4, and S6 was confirmed by the appearance of C=O stretching band at 1757 cm^{-1} , $-\text{CH}_2$ bend-

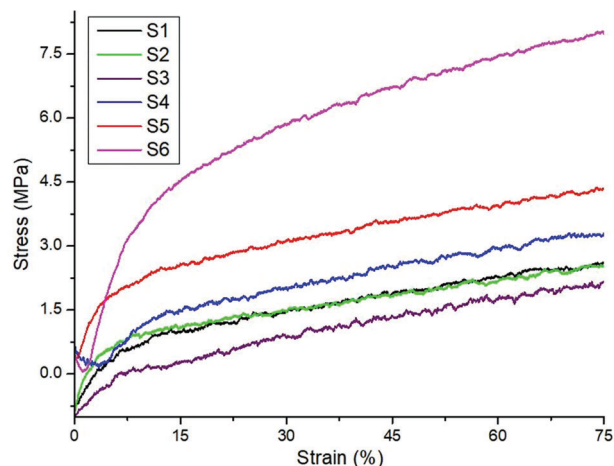


Figure 3. Representative stress–strain curves of the nanofibrous membranes (S1–S6).

ing vibrations at 1453 cm^{-1} , C–O–C stretching band at 1200 and 1083 cm^{-1} , and a short peak at 872 cm^{-1} . These peaks are in accordance with the characteristic peaks of pure PLA that appears at 1757 , 1453 , 1268 , and 868 cm^{-1} . These results are in agreement with the results in the literature.^[53] This slight change shows that the interaction between the polymer and drug was very weak. SF on the other hand shows the absorption peaks at 1620 , 1508 , and 1235 cm^{-1} which are visible in formulations S5 and S6 at positions 1650 , 1532 , and 1238 cm^{-1} . It was noted that there was a shift from a more β -sheet rich structure when SF is blended with PCL, as compared to a more amorphous state when SF is blended with PLA which may be due to subtle differences in hydrogen bonding interactions between the esters in the PCL/PLA and amides in the SF. The presence of CFX was confirmed by the carbonyl stretches (C–O) at 1720 – 1750 cm^{-1} and N–O stretching at 1350 – 1425 cm^{-1} .

The mechanical properties of the mats were investigated by tensile testing and the stress–strain curves of the mats (S1–S6) are shown in **Figure 3**. A similar tensile pattern is exhibited by the membranes with subtle differences in magnitude. The mats showed a proportional increase in the stress–strain curve below 5% strain with a visible increase in the case of samples S5 and S6, with subsequent variation until the ultimate tensile strength is reached. This increase in the tensile strength is attributed to the presence of SF.^[32,54] The membranes exhibited an ultimate tensile strength of 4.44, 4.46, 6.13, 7.17, 8.14, and 9.38 MPa with an increasing order followed for samples as $\text{S1} < \text{S2} < \text{S4} < \text{S3} < \text{S5} < \text{S6}$. The mats were able to resist the elongation at break up to 75% after which they failed at various points (the plot areas do not show the post fracture behavior). The length of the mats almost doubled from their original lengths. The low yield of elastic modulus in case of PLA incorporation into PCL increases the stiffness of the nanofiber strips which was also previously reported elsewhere.^[29] It is also documented that the improved mechanical properties of composite PCL/PLA nanofibers resulted from the existence of attractive forces like van der Waal forces between PCL and PLA and the slippage of both polymers during stretching/elongation.^[55] The increased load resistance between the two polymers indicates a synergistic effect improv-

Table 3. Water contact angle of the nanofiber formulations (S1–S6) \pm standard deviation (S).

Sample number	Formulation	Contact angle [°]
1	S1	110.8 \pm 0.3
2	S2	108.6 \pm 0.6
3	S3	114.2 \pm 0.6
4	S4	122.0 \pm 0.4
5	S5	77.7 \pm 0.4
6	S6	95.1 \pm 0.7

ing the toughness and reducing the brittleness of pristine PLA nanofibers.^[56] The inclusion of variable amounts of drug can also affect the intermolecular attractions between the polymers. Interestingly this factor was omitted here by keeping the weight ratio of drug constant. The addition of SF increases the breaking stress in both PCL/SF and PLA/SF membranes in a similar fashion as previously reported.^[34] The data regarding mechanical properties suggest that the tissue scaffolds are suitable for soft tissue engineering applications (including cartilage tissues).^[57–59]

Contact angle measurements offer insights into the adsorption of species from solution or indeed the behavior of cells on them. The samples studied had a hydrophobic character with angles above 70° (Table 3), due to the presence of hydrophobic PCL and PLA and hydrophilic SF. The respective contact angles can be observed in Figure 4, where the highest angle was exhibited by S4, i.e., 122° \pm 0.4°. The increasing order of contact angle measured for nanofiber sheets is S5 < S6 < S2 < S3 < S4 with angles mea-

sured as 77.76° \pm 0.39°, 95.10° \pm 0.74°, 108.6° \pm 0.62°, 114.16° \pm 0.55°, and 122° \pm 0.4° respectively. It is evident from the results that the overall nature of nanofibers remained hydrophobic and only the degree of hydrophobicity is changed.

3.2. In Vitro Drug Release

Among the various factors involved in the diffusion of drug from a polymeric carrier are solubility, swelling, and wettability of the polymer matrix in the testing medium. It is assumed that the release mechanism from these nanofibers is most likely diffusion controlled rather than swelling controlled or triggered.^[46] Figure 5 shows the drug release profile of all formulations (S2–S6). An initial burst release was observed ascribed to the surface desorption and lack of a proper diffusion barrier, however, the overall percentage released changed for each of the different formulations. Sample S2 has shown the slowest release of drug in the release medium with 4.0% \pm 0.2% of drug release after 2 h. Similarly sample S3 and S4 has resulted in 9.6% \pm 2.3% and 7.5% \pm 3.7% of the drug release, respectively. A uniform increase in drug release can be seen after 6 h where 9.0% \pm 3.4%, 16% \pm 4.5%, and 13% \pm 4.0% of the total drug contents were released by formulations S2, S3, and S4, respectively. This very slow drug release was due to the hydrophobic and slow erodible nature of both PCL and PLA. The cumulative drug release from these formulations becomes slower with time and after placement for 72 h in the dissolution medium was noted as 29%, 47%, and 40% respectively.

Polymer type and concentration along with other experimental parameters can drastically affect drug release. Slow erosion of

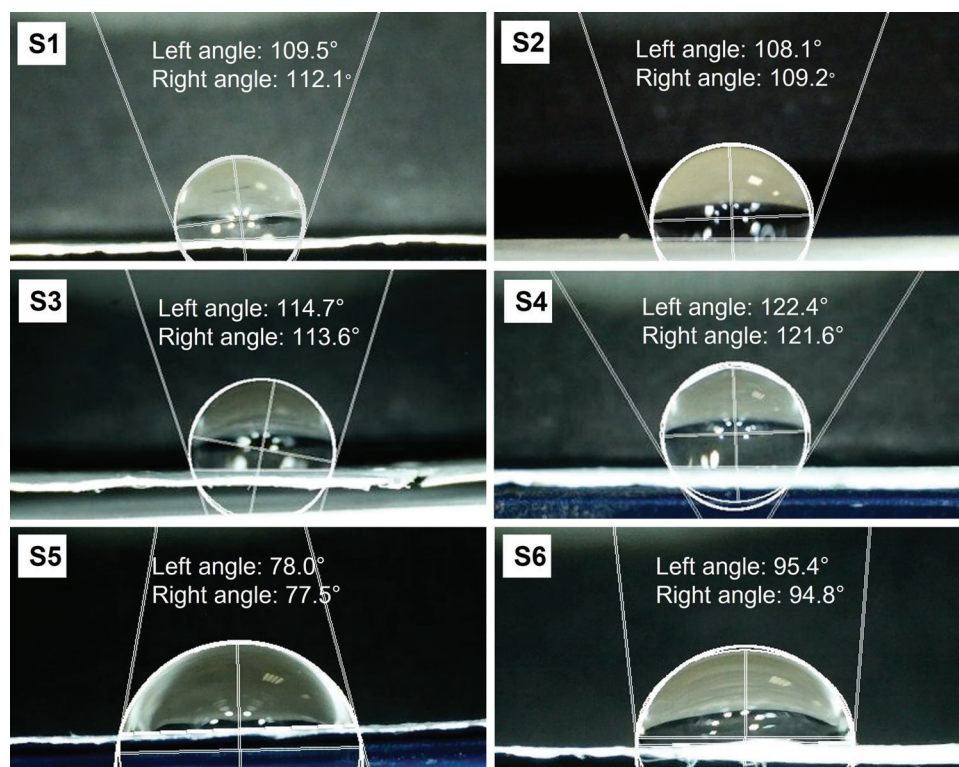


Figure 4. Water contact angle of the nanofiber formulations (S1–S6).

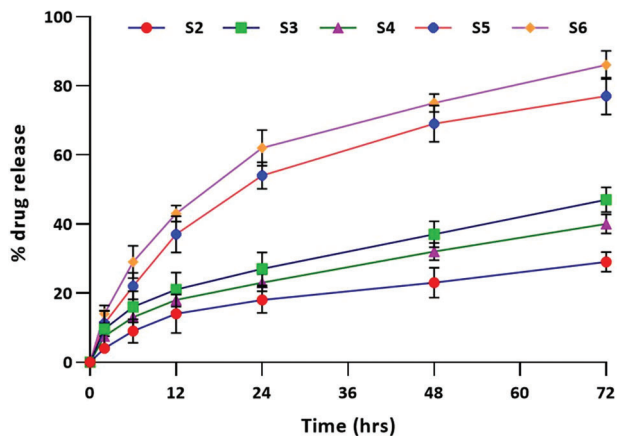


Figure 5. In vitro drug release profile of nanofiber formulations (S2–S6).

Table 4. Drug release kinetics of the nanofiber mats.

Code	Zero order	First order	Higuchi R^2	Hixson Crowell	Korsmeyer Peppas n
S2	0.8830	0.5608	0.9893	0.9032	0.707
S3	0.9039	0.4786	0.9947	0.9374	0.729
S4	0.9068	0.5101	0.9969	0.9340	0.717
S5	0.8602	0.4720	0.9819	0.9330	0.872
S6	0.8411	0.4323	0.9786	0.9417	0.870

the polymer is characterized by a slow diffusion of drug from the polymer core to the surface hence lesser drug availability in the dissolution medium.^[52] On the contrary, a systematic increase in drug release for formulation S5 and S6 was noted after 2 h, i.e., $11.2\% \pm 3.7\%$ and $14.0\% \pm 2.5\%$, respectively. These results are relatable to the presence of hydrophilic domains in the SF backbone which improves overall wettability of the samples allowing the fluid to enter the microchannels thus releasing more drug. After 6 h formulation S5 released $22.0\% \pm 3.9\%$ and S6 released $29.0\% \pm 4.8\%$ which is much more as compared to formulations S2, S3, and S4. Among the formulations the maximum drug release after 72 h was exhibited by formulation S5 and S6 by releasing most of their drug load into the dissolution medium. S5 has resulted in $77.0\% \pm 5.4\%$ drug release and S6 has resulted in $86.0\% \pm 4.1\%$ drug release.

To find out the mechanism of drug release from the mats, various kinetic models were applied on the obtained drug release data as shown in Table 4. It can be seen that the value of R^2 was on the lower side and far away from one in case of First order release model which shows that the release from these nanofibers was not independent of the concentration of drug. The representative values of R^2 for zero order release in case of S2, S3, S4, S5, and S6 were 0.883, 0.903, 0.906, 0.860, and 0.841, respectively.

3.3. Antibacterial Activity

The antibacterial effect of obtained nanofiber mats was measured against two common human pathogenic strains, *S. aureus* and *E. coli*. To confirm whether CFX-loaded nanofibers display effective

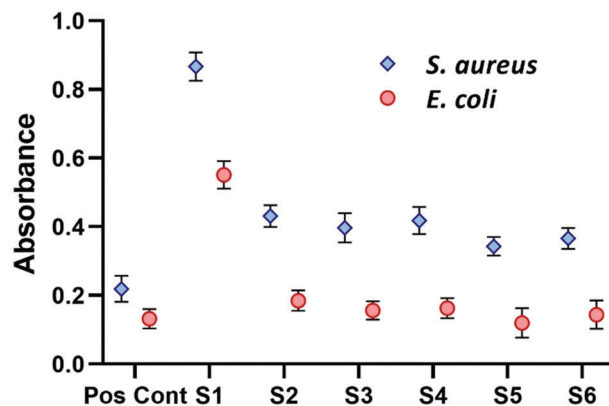


Figure 6. UV-vis absorbance of drug loaded nanofibers against *S. aureus* and *E. coli*.

Table 5. Zone of inhibition of CFX-loaded nanofiber mats against *S. aureus* and *E. coli*.

Sample code ^{a)}	<i>S. aureus</i> (ATCC-6538)	<i>E. coli</i> (ATCC-25922)
ZOI [mm]		
Pos Cont.	20.0 ± 1.0	41.0 ± 1.7
S1	0	0
S2	12.7 ± 1.0 ****	33.7 ± 1.5 ****
S3	14.7 ± 2.0 ****	36.3 ± 0.6 ****
S4	13.6 ± 2.1 ****	35.8 ± 1.1 ****
S5	14.0 ± 1.6 ****	35.3 ± 1.2 ****
S6	17.3 ± 1.6 ****	37.3 ± 2.1 ****

^{a)} Values are shown as mean \pm SD ($n = 3$), **** $p < 0.0001$.

antibacterial activity, unloaded PCL nanofibers were used as negative control, while CFX was used as a reference positive control. Turbidity of the bacterial suspensions was used to compare bacterial viability (higher turbidity correlated suggests less antibacterial effect). Figure 6 shows that the UV-vis absorption intensity for *S. aureus* is greater than for *E. coli* because of the increased sensitivity of *E. coli* toward CFX. The increased absorption intensity of negative control shows that the bacterial colonies survived in the absence of antibiotic, whereas the positive control has lowest absorbance value as the drug was readily available for bacteriostatic effect. From these results it is clear that all samples possess antibacterial potential; however, the slow release of drug from pristine PCL and PLA nanofibers resulted in increased absorption than those samples where SF is blended with these polymers.

The diameter of the zone of inhibition around nanofiber mats against both *S. aureus* and *E. coli* is shown in Table 5. The reference positive control displayed highest zone of inhibition, i.e., 20.0 ± 1.0 and 41.0 ± 1.7 mm against *S. aureus* and *E. coli*, respectively. The nanofibers effectiveness was considerably higher against *E. coli* than *S. aureus* due to its sensitivity toward CFX. Analysis of variance (ANOVA) has confirmed that the results are showing a significant ($p < 0.0001$) reduction in bacterial growth as compared to the control however, a nonsignificant difference ($p \geq 0.05$) was noted when intergroup comparison was made.

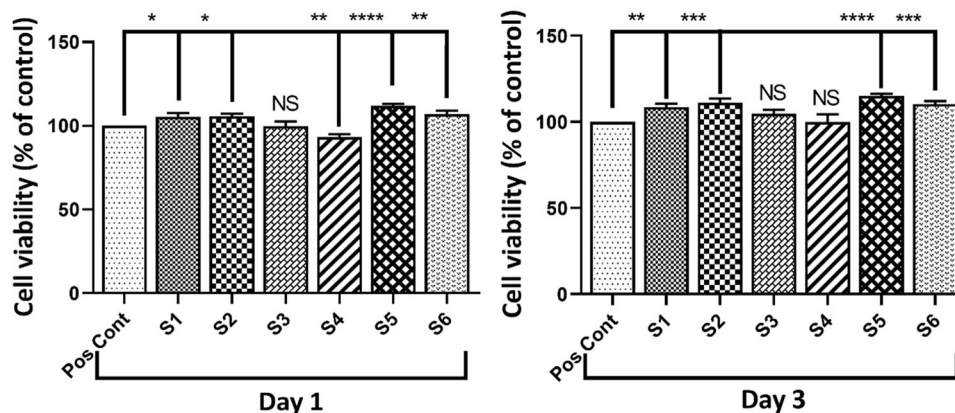


Figure 7. MTT analysis of the drug loaded electrospun mats (S1–S6). Error bars represents mean \pm SD ($n = 3$), * $p < 0.05$, ** $p < 0.005$, *** $p < 0.001$, **** $p < 0.0001$.

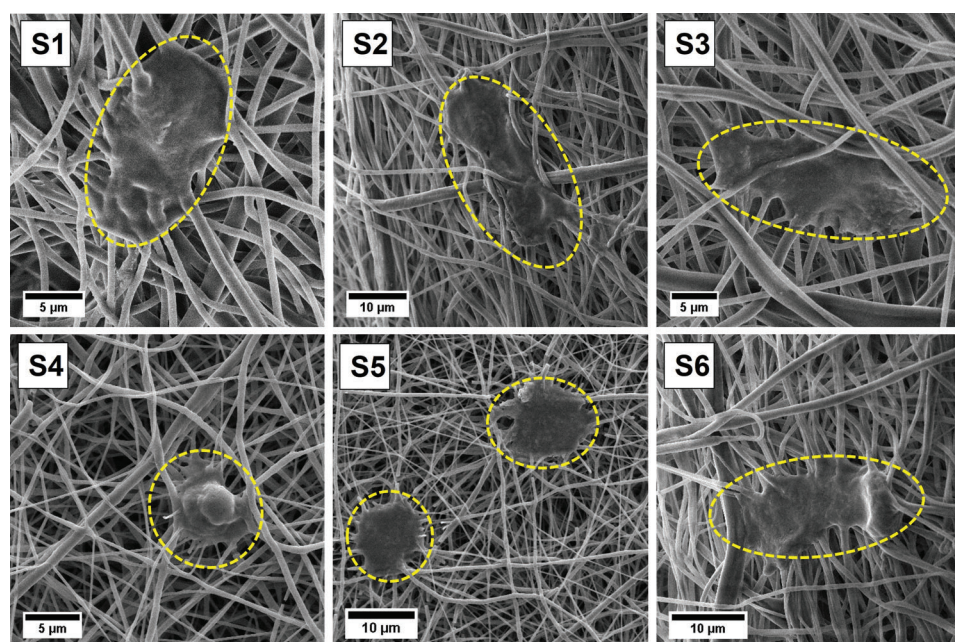


Figure 8. SEM micrographs showing morphologies of NIH-3T3 cells (S1–S6) after 3 d of culture.

Among all the samples tested, S6 has shown a significant reduction ($p < 0.0001$) in bacterial growth with a round inhibition area covering 17.3 ± 1.6 and 37.3 ± 2.1 mm against *S. aureus* and *E. coli*, respectively. This highest inhibition results from the rapid drug diffusion into the growth medium which can also be related to the drug release profile where the drug release was high in the case of S6.

3.4. Cell Viability

The viability of NIH-3T3 fibroblast cells was assessed by MTT assay analysis with respect to incubation time (day 1 and day 3) is shown in **Figure 7**. The cells grown on bare tissue culture plate were used as controls. A statistically significant ($p < 0.05$) increase in cell growth was noted in S1 and S2 after day 1 as com-

pared to the control, i.e., $105.5\% \pm 2.1\%$ and $105.5\% \pm 1.7\%$ respectively. A slight but nonsignificant decrease in cell viability was noted for S3, i.e., $99.6\% \pm 2.9\%$ whereas a significant decrease ($p < 0.01$) was displayed by S4, i.e., $93.2\% \pm 1.7\%$. On the contrary, S5 and S6 has shown a significant increase in cell viability, i.e., $111.8\% \pm 1.2\%$ ($p < 0.0001$) and $106.89\% \pm 2.2\%$ ($p < 0.01$), respectively. The same samples were incubated for another 48 h and again the cell viability was estimated where all samples have shown considerable improvement in cell growth as compared to positive control. Samples S1, S2, S5, and S6 has shown significantly improved cell growth as compared to control with cell viability values of $108.6\% \pm 1.9\%$ ($p < 0.01$), $111.1\% \pm 2.5\%$ ($p < 0.001$), $115.1\% \pm 1.2\%$ ($p < 0.0001$), and $110.4\% \pm 1.7\%$ ($p < 0.001$), respectively. Cell growth of S3 and S4 was also improved but nonsignificantly with values $104.7\% \pm 2.4\%$ and $99.9\% \pm 4.4\%$, respectively. From these results it is evident that

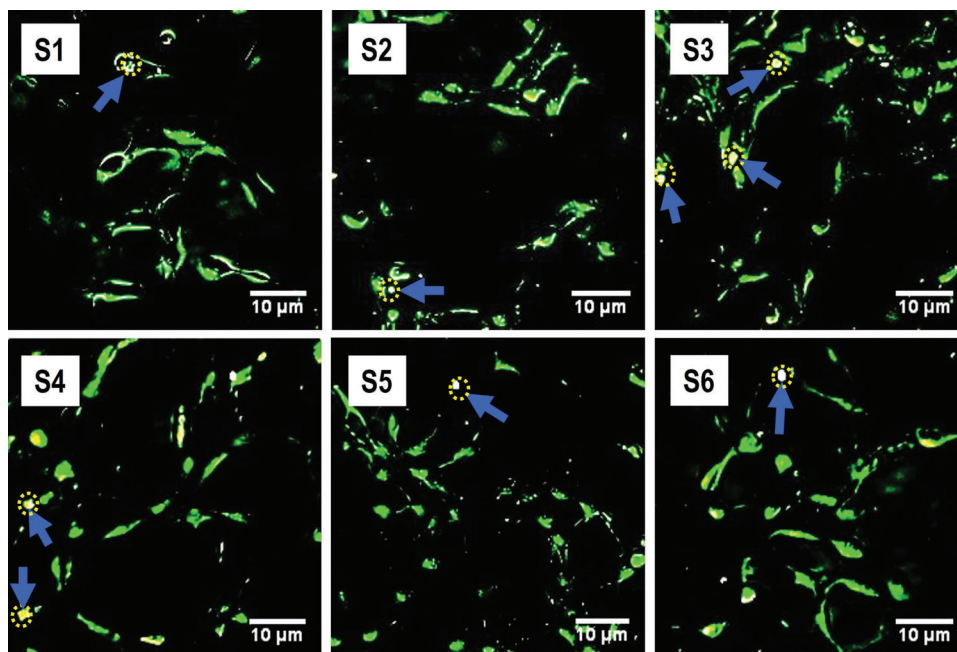


Figure 9. Live–dead assay of the drug loaded nanofibers (S1–S6) after 3 d incubation.

wettability has an important role in cell attachment and viability by preferentially adsorbing the cell adhesive proteins.

3.5. Cell Adhesion and Proliferation

Cell attachment assay was performed to observe the interaction and morphology of attached cells using SEM. The results shown in **Figure 8** highlight the clusters of NIH-3T3 cells adhered to the nanofibers, showing excellent connection between the 3D structured nanofibers and cultured cells (broken fibers around the cells can be seen in **Figure 8**, plausibly due to sample handling or cell-induced changes). The attached cells show polygonal extension of the cytoplasm rather unidirectional elongation which is due to the random spinning of nonwoven fibers instead of aligned fibers.^[60] The increased cell density after 3 d of culture confirms cell proliferation. A live–dead assay (**Figure 9**) was used to confirm the presence of live cells (represented by green color) on the mats in all samples, the small number of dead cells in samples are highlighted by blue arrowheads. These results are in accordance with the previously reported biocompatibility of polymers such as PCL, PLA, and SF.^[27,36,61–63]

4. Conclusion

A series of nanofiber formulations incorporating CFX and polymers such as PCL, PLA, SF, and composites of mixtures thereof were prepared by electrospinning. The electrospun fibers in the nanofiber mats were fairly smooth with diameters typically ≤ 500 nm; the electrospun mats had interconnected pores, were slightly hydrophobic, and had mechanical properties analogous to cartilage tissue. PCL/PLA based nanofibers were more elastic and displayed controlled release of CFX, this can be correlated

with the antibacterial profile where the initial burst release of the drug from the nanofibers containing SF displayed the highest zone of inhibition (with a correlation between sample hydrophobicity and drug release profiles). Cells were observed to adhere and proliferate on all samples, and such biomaterials (or variations thereof) have long-term potential for application as scaffolds for cartilage tissue engineering.

Acknowledgements

M.S. and J.G.H. acknowledge financial support from the Pakistan Higher Education Commission (HEC), International Research Support Initiative Program. A.F.K. acknowledges financial support from the HEC Pakistan under the National Research Programme for Universities (NRPU) project scheme (Grant No. 4099).

Conflict of Interest

The authors declare no conflict of interest.

Data Availability Statement

The data that support the findings of this study are available from the corresponding author upon reasonable request.

Keywords

antibacterial, cartilage, composite, drug delivery, electrospinning

Received: May 31, 2022
Revised: June 30, 2022
Published online:

- [1] M.-C. Laiguillon, A. Courties, X. Houard, M. Auclair, A. Sautet, J. Ca-
peau, B. Fève, F. Berenbaum, J. Sellam, *Osteoarthrotic Cartilage* **2015**,
23, 1513.
- [2] J. Neumann, F. C. Hofmann, U. Heilmeier, W. Ashmeik, K. Tang, A.
S. Gersing, B. J. Schwaiger, M. C. Nevitt, G. B. Joseph, N. E. Lane, C.
E. Mcculloch, T. M. Link, *Osteoarthrotic Cartilage* **2018**, 26, 751.
- [3] X. Ren, J. Li, J. Li, Y. Jiang, L. Li, Q. Yao, Q. Ke, H. Xu, *Chem. Eng. J.*
2019, 370, 1027.
- [4] R. Zheng, H. Duan, J. Xue, Y. Liu, B. Feng, S. Zhao, Y. Zhu, Y. Liu, A.
He, W. Zhang, W. Liu, Y. Cao, G. Zhou, *Biomaterials* **2014**, 35, 152.
- [5] P. Lee, K. Tran, W. Chang, N. B. Shelke, S. G. Kumbar, X. Yu, *J. Biomed.*
Nanotechnol. **2014**, 10, 1469.
- [6] W. Chen, C. Wang, Y. Gao, Y. Wu, G. Wu, X. Shi, Y. Du, H. Deng, *Car-*
bohydr. Polym. **2020**, 229, 115544.
- [7] L. Xiao, M. Wu, F. Yan, Y. Xie, Z. Liu, H. Huang, Z. Yang, S. Yao, L. Cai,
Int. J. Biol. Macromol. **2021**, 172, 19.
- [8] Z. Li, P. Liu, T. Yang, Y. Sun, Q. i You, J. Li, Z. Wang, B. Han, *J. Biomater.*
Appl. **2016**, 30, 1552.
- [9] B. J. Huang, J. C. Hu, K. A. Athanasiou, *Biomaterials* **2016**, 98, 1.
- [10] T. Zhao, Z. Wei, W. Zhu, X. Weng, *Bioengineering* **2022**, 9, 132.
- [11] R. Censi, A. Dubbini, P. Matricardi, *Curr. Pharm. Des.* **2015**, 21, 1545.
- [12] J. C. Silva, R. N. Udangawa, J. Chen, C. D. Mancinelli, F. F. Garrudo,
P. E. Mikael, J. M. S. Cabral, F. C. Ferreira, R. J. Linhardt, *Mater. Sci.*
Eng., C **2020**, 107, 110291.
- [13] E. N. Yilmaz, D. I. Zeugolis, *Front. Bioeng. Biotechnol.* **2020**, 8, 77.
- [14] Y. Liu, M. Hao, Z. Chen, L. Liu, Y. Liu, W. Yang, S. Ramakrishna, *Curr.*
Opin. Biomed. Eng. **2020**, 13, 174.
- [15] F. Mohammadian, A. Eatemadi, *Artif. Cells, Nanomed., Biotechnol.*
2017, 45, 881.
- [16] S. Homaeigohar, A. R. Boccaccini, *Acta Biomater.* **2020**, 107, 25.
- [17] O. Janoušková, *Physiol. Res.* **2018**, 67, S335.
- [18] S. D. McCullen, H. Autefage, A. Callanan, E. Gentleman, M. M.
Stevens, *Tissue Eng., Part A* **2012**, 18, 2073.
- [19] U. Aggarwal, A. K. Goyal, G. Rath, *Mater. Sci. Eng., C* **2017**, 75, 125.
- [20] K. Ye, H. Kuang, Z. You, Y. Morsi, X. Mo, *Pharmaceutics* **2019**, 11, 182.
- [21] Y. Ning, W. Shen, F. Ao, *RSC Adv.* **2020**, 10, 37246.
- [22] V. Pertici, G. Martrou, D. Gígmés, T. Trimaille, *Curr. Med. Chem.* **2018**,
25, 2385.
- [23] C. I. Idumah, *Polym. Polym. Compos.* **2021**, 29, 509.
- [24] S. Farzambar, M. Naseri-Nosar, H. Sahraeyma, A. Ehterami, A.
Goodarzi, M. Rahmati, G. Ahmadi Lakalayeh, S. Ghorbani, A. Vaez,
M. Salehi, *Int. J. Polym. Mater. Polym. Biomater.* **2019**, 68, 472.
- [25] S. Mohandesnezhad, Y. Pilehvar-Soltanahmadi, E. Alizadeh, A.
Goodarzi, S. Davaran, M. Khatamian, N. Zarghami, M. Samiei, M.
Aghazadeh, A. Akbarzadeh, *Mater. Chem. Phys.* **2020**, 252, 123152.
- [26] D. W. Y. Toong, H. W. Toh, J. C. K. Ng, P. E. H. Wong, H. L. Leo, S.
Venkatraman, L. P. Tan, H. Y. Ang, Y. Huang, *Int. J. Mol. Sci.* **2020**, 21,
3444.
- [27] L. Wang, C. Wang, L. Zhou, Z. Bi, M. Shi, D. Wang, Q. Li, *Eur. Polym.*
J. **2021**, 161, 110834.
- [28] M. Herrero-Herrero, S. Alberdi-Torres, M. L. González-Fernández, G.
Vilariño-Feltrer, J. C. Rodríguez-Hernández, A. Vallés-Lluch, V. Villar-
Suárez, *Polym. Test.* **2021**, 103, 107364.
- [29] T. Xu, Q. Yao, J. M. Miszuk, H. J. Sanyour, Z. Hong, H. Sun, H. Fong,
Colloids Surf., B **2018**, 171, 31.
- [30] R. Sridhar, R. Lakshminarayanan, K. Madhaiyan, V. Amutha Barathi,
K. H. C. Lim, S. Ramakrishna, *Chem. Soc. Rev.* **2015**, 44, 790.
- [31] P. Mostafavi, M. Naeimi, *Mater. Technol.* **2021**, 1329.
- [32] M. A. Nazeer, E. Yilgor, I. Yilgor, *Polymer* **2019**, 168, 86.
- [33] T. Roy, P. Maity, A. Rameshbabu, B. Das, A. John, A. Dutta, S. Ghorai,
S. Chattopadhyay, S. Dhara, *Bioengineering* **2018**, 5, 68.
- [34] Z. Wang, X. Song, Y. Cui, K. Cheng, X. Tian, M. Dong, L. Liu, *J. Colloid*
Interface Sci. **2021**, 593, 142.
- [35] M. Farokhi, F. Mottaghitalab, Y. Fatahi, M. R. Saeb, P. Zarrintaj, S. C.
Kundu, A. Khademhosseini, *Eur. Polym. J.* **2019**, 115, 251.
- [36] G. Cheng, Z. Davoudi, X. Xing, X. Yu, X. Cheng, Z. Li, H. Deng, Q.
Wang, *ACS Biomater. Sci. Eng.* **2018**, 4, 2704.
- [37] W. Sun, D. A. Gregory, M. A. Tomeh, X. Zhao, *Int. J. Mol. Sci.* **2021**,
22, 1499.
- [38] F. A. Sheikh, H. W. Ju, J. M. Lee, B. M. Moon, H. J. Park, O. J. Lee, J.-H.
Kim, D.-K. Kim, C. H. Park, *Nanomed. Nanotechnol. Biol. Med.* **2015**,
11, 681.
- [39] C. Belbéoch, J. Lejeune, P. Vroman, F. Salaün, *Environ. Chem. Lett.*
2021, 19, 1737.
- [40] J. G. Hardy, T. R. Scheibel, *Prog. Polym. Sci.* **2010**, 35, 1093.
- [41] S. Tandon, B. Kandasubramanian, S. M. Ibrahim, *Ind. Eng. Chem. Res.*
2020, 59, 17593.
- [42] R. Mirshahi, M. Sardarinia, N. Nilforushan, *Am. J. Ophthalmol. Case*
Rep. **2020**, 20, 100903.
- [43] E. Ramírez-Cedillo, W. Ortega-Lara, M. Rocha-Pizaña, J. Gutierrez-
Uribe, A. Elías-Zúñiga, C. Rodríguez, *Membranes* **2019**, 9, 12.
- [44] S. M. Atyabi, F. Sharifi, S. Irani, M. Zandi, H. Mivehchi, Z. Nagheh,
Cell Biochem. Biophys. **2016**, 74, 181.
- [45] J.-W. Song, L.-W. Fan, *Adv. Colloid Interface Sci.* **2021**, 288, 102339.
- [46] Z. Sultanova, G. Kaleli, G. Kabay, M. Mutlu, *Int. J. Pharm.* **2016**, 505,
133.
- [47] L. M. Da Silva, H. R. N. Salgado, *J. Microbiol. Methods* **2015**, 110,
49.
- [48] P. Zahedi, Z. Karami, I. Rezaeian, S.-H. Jafari, P. Mahdaviani, A. H.
Abdolghaffari, M. Abdollahi, *J. Appl. Polym. Sci.* **2012**, 124, 4174.
- [49] E. Naghashzargar, S. Farè, V. Catto, S. Bertoldi, D. Semnani, S. Kar-
basi, M. C. Tanzi, *J. Appl. Biomater. Funct. Mater.* **2015**, 13, 156.
- [50] M. J. Mochane, T. S. Motsoeneng, E. R. Sadiku, T. C. Mokhena, J. S.
Sefadi, *Appl. Sci.* **2019**, 9, 2205.
- [51] M. O. Aydogdu, E. Altun, J. Ahmed, O. Gunduz, M. Edirisinghe,
Polym. Polym. Compos. **2019**, 11, 1148.
- [52] S.-F. Chou, D. Carson, K. A. Woodrow, *J. Controlled Release* **2015**, 220,
584.
- [53] F. Sharif, S. Tabassum, W. Mustafa, A. Asif, F. Zarif, M. Tariq, S. A. Sid-
diqui, M. A. Gilani, I. Ur Rehman, S. Macneil, *Polym. Compos.* **2019**,
40, 1564.
- [54] H. Yuan, H. Shi, X. Qiu, Y. Chen, *J. Biomater. Sci., Polym. Ed.* **2016**, 27,
263.
- [55] Y. Lu, Y.-C. Chen, P.-H. Zhang, *Fibres Text. East. Eur.* **2016**, 24, 17.
- [56] Y. Wang, Y. Wang, Q. Wei, J. Zhang, M. Lei, M. Li, D. Li, *J. Polym. Res.*
2021, 28, 451.
- [57] G. Singh, A. Chanda, *Biomed. Mater.* **2021**, 16, 062004.
- [58] M. Setayeshmehr, E. Esfandiari, M. Rafieinia, B. Hashemibeni, A.
Taheri-Kafrani, A. Samadikuchaksaraei, D. L. Kaplan, L. Moroni, M.
T. Joghataei, *Tissue Eng., Part B* **2019**, 25, 202.
- [59] J. M. Patel, B. C. Wise, E. D. Bonnevie, R. L. Mauck, *Tissue Eng., Part*
C **2019**, 25, 593.
- [60] G.-F. Liu, D. Zhang, C.-L. Feng, *Angew. Chem., Int. Ed.* **2014**, 53, 7789.
- [61] N. H. Marei, I. M. El-Sherbiny, A. Lotfy, A. El-Badawy, N. El-Badri, *Int.*
J. Biol. Macromol. **2016**, 93, 9.
- [62] Q. Yao, J. G. L. Cosme, T. Xu, J. M. Miszuk, P. H. S. Picciani, H. Fong,
H. Sun, *Biomaterials* **2017**, 115, 115.
- [63] R. R. Mallepally, M. A. Marin, V. Surampudi, B. Subia, R. R. Rao, S. C.
Kundu, M. A. Mchugh, *Biomed. Mater.* **2015**, 10, 035002.